Experimental and thermodynamic analyses of a novel anode supported solid oxide fuel cell

Ahmed Khaled ElKashat
Department of Mechanical Engineering
University of Alberta
Edmonton, Canada
elkashat@ualberta.ca

Amir Reza Hanifi
Department of Chemical & Material Engineering
Department of Mechanical Engineering
University of Alberta
Edmonton, Canada
hanifi@ualberta.ca

Amir Reza Razmi
Department of Mechanical Engineering
University of Alberta
Edmonton, Canada
razmi@ualberta.ca

Thomas H. Etsell
Department of Chemical & Material Engineering
University of Alberta
Edmonton, Canada
tetsell@ualberta.ca

Sajad Vafaeenezhad
Department of Chemical & Material Engineering
University of Alberta
Edmonton, Canada
sajad.vafaeenezhad@ualberta.ca

Mahdi Shahbakhti
Department of Mechanical Engineering
University of Alberta
Edmonton, Canada
mahdi@ualberta.ca

***Abstract*—Solid oxide fuel cell (SOFC) is a promising clean technology to generate power with high efficiency at different scales. Decreasing the degradation rate of SOFCs is a challenge that can be tackled by lowering the operation temperature ($<$ 650°C). However, this can adversely affect cell performance and therefore it is important to develop novel electrodes which show high performance at low operation temperatures. This paper presents a novel anode-supported tubular fuel cell consisting of NiO:YSZ (65:35 wt%) cermet with 30 vol.% graphite as the pore-former. The anode support was coated with a thin anode functional layer (20 µm) with a NiO:YSZ ratio of 65:35 wt%. The Ruddlesden-Popper cathode ($Nd_2NiO_{4+\delta}$) microstructure was composed of nano-size ($\leq$ 50 nm) particles infiltrated into a thin porous YSZ scaffold. The combination of using a thing dense YSZ electrolyte (6.5 µm), an active anode functional layer, and a high-performing cathode led to high performance at low temperatures. The proposed cell was analyzed both experimentally and thermodynamically at three temperatures of 500, 550, and 600°C. The simulation results indicate that a maximum power density of 0.1, 0.25, and 0.66 W/cm^2 can be achieved at 500, 550, and 600°C, respectively. The simulated data show an excellent match ($< 3\%$ difference) with the experimental data. This paper includes the development of an SOFC model for detailed analysis of the variables that are difficult to measure during experiments.**

***Index Terms*—Solid oxide fuel cell; SOFC; simulation; Cell polarization; Temperature effects.**

I. Introduction

The advancement of living standards and global digital transformation have led to ever-increasing electricity consumption in recent decades, resulting in the highest fossil fuel consumption and greenhouse gas (GHG) emissions in human history [1]. According to a recent report by the International Energy Agency (IEA), the energy sector accounts for the highest rate of GHG emissions nowadays. Therefore, to drastically decrease the global carbon dioxide emissions to net-zero by 2050, a significant transition in the energy sector is required [2]. In this regard, most studies have focused on the development of highly efficient, clean, and environmentally friendly renewable energy resources [3]. Fuel cell technology provides an efficient way to utilize energy by the direct conversion of the chemical energy of low-carbon (such as methane) or zero-carbon (hydrogen) fuels to electrical energy. Among different types of fuel cells, the solid oxide fuel cell (SOFC) is the most efficient, scalable, and most versatile electrochemical energy conversion system [4]. The operation temperature of the SOFC (550-850°C) makes it an ideal choice for coupling with auxiliary cycles to improve its efficiency as a combined heat and power (CHP) unit.

Anode-supported SOFC is the most common configuration of SOFCs because of its advantages such as high electrochemical performance, economic feasibility, and high mechanical stability. In spite of the better mechanical strength of cells with a thicker anode, the concentration polarization resistance increases with cell thickness due to a longer path for gas diffusion and removal of the reaction products [5]. Coating an Anode functional layer (AFL) with an engineered microstructure not only improves the active triple phase boundary (TPB) length at the anode electrochemical reaction sites but also reduces the mismatch in thermal expansion coefficients between

the anode and electrolyte interfaces. This leads to a decrease in contact and ohmic resistances, and consequently, improves cell performance. During the cell reduction, the porous nickel oxide-yttria stabilized zirconia (NiO-YSZ) anode is reduced to nickel-yttria stabilized zirconia (Ni-YSZ) to improve the electrode porosity and electrical conductivity. However, extra pore formers such as graphite, carbon black, or starch are added to the support composition for better diffusion of the fuel gas and removal of by-products from the cell [6].

Recent studies have introduced different methods to increase the efficiency of SOFCs. Haslam et al. [7] showed that cell performance is improved by increasing the anode support porosity. However, they emphasized that cell performance decreases when the TPB length decreases due to the increase of pore content in the microstructure of the functional layer. Ma et al. [8] developed a model for analyzing mass transport in the SOFC by using a thermodynamically consistent model for the prediction of the low open-circuit voltage. They concluded that the performance improved by increasing the porosity and pore diameter and decreasing the thickness and tortuosity in the support. Baek et al. [9] developed a comprehensive three-dimensional model for planar, anode-supported,and intermediate-temperature SOFCs. Their results indicated that the model was sufficiently accurate to optimize operation conditions, microstructure properties, and cell geometry.

Although the Ni-YSZ based SOFC has many advantages like low investment cost and great catalytic performance, high degradation rate is still a major challenge and further research is required. Recent studies have focused on research and development of new cells with a low degradation rate. This paper proposes a novel fuel cell that can work with high efficiency at operation temperatures as low as 500°C. Low-temperature SOFCs can reduce degradation rates significantly by operating at temperatures below 650°C; however, they require more conductive and thinner electrolytes for reducing ohmic polarization. Moreover, a tailored nano-size microstructure is required to reduce activation polarization particularly in the ceramic cathode which has lower mixed electronic and ionic conductivity and catalytic activity compared with the Ni-YSZ cermet. Ruddlesden-Popper cathode microstructure is composed of fine ($\leq$ 50 nm) infiltrated particles with high catalytic activity. Such particles are infiltrated into a thin porous YSZ layer ($<$ 20 μm) as catalysts for the oxygen reduction reaction (ORR). The above factors along with a thin and dense YSZ electrolyte and suitable adhesion between the AFL/YSZ layers resulted in a high cell performance at low temperatures in the current research. Performance of the cell was analyzed from thermodynamic point of view and validated with the experimental data. The novelty of the current study is related to the fuel cell design as well as simulation of the electrochemical performance of the SOFC by analyzing the associated polarizations.

II. CELL DESIGN AND EXPERIMENTS

Slip casting was used for fabrication of the anode support. Details of the slip casting process are explained elsewhere [10]. In brief, NiO (J.T. Baker, 250 nm average particle size) was mixed with YSZ (Tosoh 8-YSZ, 250 nm average particle size) with a 65:35 wt% ratio. Powders were added to water (1:1 ratio) and milled for 3h using a rotary ball mill. Afterward, extra water was added to reduce the solid loading to 40% and the pH of the suspension was set to 4.0 using hydrochloric acid to achieve a stable suspension. Graphite (4.5 μm, average particle size) was added to the suspension as a pore former and milled again for 15 minutes. The suspension was slip cast into plaster molds and semi-dried tubes were removed from the molds. Support tubes were pre-sintered at 950°C for 3h.

AFL was coated onto the pre-sintered supports using dip-coating technique. NiO and YSZ (NiO:YSZ = 65:35 wt%) were added to ethanol and binder (6 wt% ethyl cellulose in terpineol) and milled for 2h using a ball mill. Supports were dipped into the AFL suspension twice and pre-sintered at 900°C for 3h following drying at room temperature. The YSZ electrolyte was coated onto the AFL using a dip coat. YSZ and ethanol (1:8 weight ratio) and binder (6 wt% ethyl cellulose in terpineol) were milled for 1h using a planetary mill (300 rpm). Then, the suspension was sonicated for three minutes, and supports were dipped once into the suspension. The coated samples were dried at room temperature and sintered at 1400°C for 3h. The same process was repeated the next day with a YSZ suspension with 1:10 weight ratio to make sure a gas-tight and thin electrolyte was achieved.

A thin YSZ scaffold was coated onto the electrolyte by dip-coating and heat-treated at 1300°C for 3h. $Nd_2NiO_{4+\delta}$ was infiltrated into the scaffold as the active cathode material. Details of the infiltration process are explained elsewhere [11]. Briefly, the infiltration solution was prepared by adding Nd and Ni nitrates with the stoichiometric ratio to water and surfactant (Menhaden fish oil). The infiltrate solution was dropwise added to the YSZ scaffold, and it was heat treated at 350°C for the nitrates to decompose. This process was repeated twice for the infiltrate solid loading to reach 30 wt% of the YSZ scaffold. A schematic diagram of the cell test setup is shown in Fig. 1 (a). Humidified hydrogen (3 vol.% H2O) with 50 sccm was fed to the cell through alumina tubes. Silver and gold pastes were coated onto the anode and cathode, respectively, and heat-treated at 200°C. A copper mesh was pushed into the anode as a second anode current collector. The fuel chamber was sealed using Ceramabond 552 paste. Air with a flow of 150 sccm was used on the cathode side. The cell was put inside the hot zone of the furnace and a temperature of the cell was controlled using a thermocouple close to the cathode.

The fabricated tubular fuel cells before testing are shown in Fig. 1 (b). Hydrogen enters the water impinger and after saturating with water vapor, reaches the furnace. Passing through the furnace, the hydrogen temperature increases before reaching the anode. The solid porous electrodes allow hydrogen and air to diffuse to the reaction sites, where the oxygen ions produced by the electrochemical reactions at the cathode are transferred to the anode side. Hydrogen diffuses from the anode to its interface with the electrolyte, where the

catalytic reaction begins, and electrons are generated through the electrochemical reactions. The low thickness of the electrolyte reduces the ohmic resistance of the cell significantly. Moreover, the infiltrated cathode with nano-size $Nd_2NiO_{4+\delta}$ particles and the fine AFL grains increase the TPB length inside the cathode and anode, reducing the polarization resistance. As a result, the SOFC can operate at lower temperatures with a higher performance.

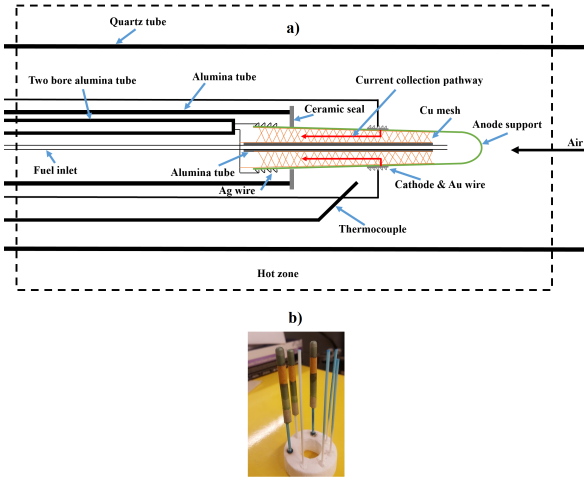

Fig. 1. a) Schematic diagram of the tubular cell inside the setup and b) image of the experimental setup.

III. MODELING

In this section, the governing equations for modeling of the proposed low-temperature SOFC based on the electrochemical and thermodynamic processes are presented. The model input parameters are listed in Table I. The thickness of the electrolyte, cathode, and anode in Table I are matched with the experimental values using the SEM (scanning electron microscope) images in Fig. 2.

TABLE I
SOFC MODEL INPUT PARAMETERS.

Parameter	Value	Unit
Active surface area	2	cm^2
Air flow rate	150	sccm
Ambient pressure	1.01	bar
Ambient temperature	298	K
Conductivity of anode	$\frac{9.5*10^7}{T} exp(-\frac{1150}{T})$	Ω m
Conductivity of cathode	$\frac{4.2*10^7}{T} exp(-\frac{1200}{T})$	Ω m
Conductivity of electrolyte	$33.4*10^3 exp(-\frac{10300}{T})$	Ω m
Transfer coefficient	0.5	–
Hydrogen flow rate	50	sccm
Faraday's constant	96485	C mol^{-1}
Fuel utilization factor	70	%
SOFC operating pressure	1.01	bar
Thickness of the anode	368	μm
Thickness of the cathode	7.5	μm
Thickness of the electrolyte	6.5	μm

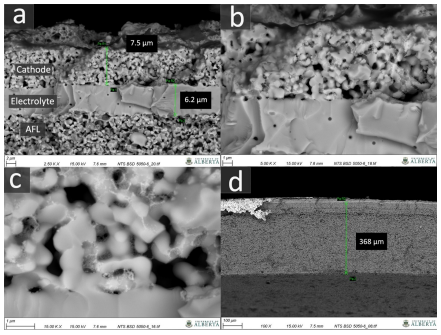

Fig. 2. Cross section SEM micrographs of the cell a) cathode, electrolyte and AFL b, c) higher magnifications of the cathode d) lower magnification, showing the total thickness of the anode electrode (support and the AFL).

A. Actual voltage

Performance of the fuel cell is characterized by the current-voltage (I-V) diagram representing the fuel cell's outlet voltage respective to different current densities. Theoretically, the voltage of a fuel cell is always lower than the ideal voltage calculated using thermodynamics laws. In addition, lower voltage values will be generated from the cell at higher current densities, restricting the overall power produced in reality [12]. The reversible cell voltage, also known as the electromotive force (emf), is determined by the difference between the thermodynamic potentials of the electrode reactions. The emf is affected by the composition of the gas and the temperature of the cell, which is stated by the Nernst Equation [13]:

$$V_{Nerst} = E^o + \frac{RT}{2F} ln \frac{P_{H2} P_{O2}^{0.5}}{P_{H2O}} \quad (1)$$

where, P_i is the partial pressure of component i, R is the universal gas constant, and T is the absolute operating temperature. E^o is the standard open-circuit voltage that is calculated as follows:

$$E^o = -\frac{\Delta G^o}{n\mathrm{F}} \quad (2)$$

ΔG^o shows the alteration of Gibbs free energy at ambient pressure, n shows the number of electrons exchanged in the reaction, and F is Faraday's constant.

When the net flowing electrical current through the fuel cell is equal to zero, the maximum achievable voltage is reached. Internal resistances and overpotential polarizations cause the cell's actual voltage to be less than the open-circuit voltage. The fuel cell polarizations are proportional to the electrical current drawn from the cell. There are three main types of polarizations, which determine a fuel cell I–V curve and its characteristic shape namely:

- Activation losses related to the electrochemical reaction.
- Ohmic losses related to the ionic and electronic conduction.
- Concentration losses related to the mass transport.

The actual output voltage of the fuel cell can be expressed by subtracting the voltage calculated based on thermodynamic

laws with the voltage drop because of the different polarizations. The SOFC's output voltage can be calculated as [13]:

$$V = V_{Nerst} - (\Delta V_{act} + \Delta V_{ohm} + \Delta V_{con}) \tag{3}$$

where, ΔV_{act}, ΔV_{ohm} and ΔV_{con} are the activation overpotential, ohmic overpotential, and concentration overpotential, respectively.

B. Ohmic polarization

Ohmic polarization is caused by the resistance to the ion flow in the electrolyte and electrodes, and the resistance of the electron flow in the electrode materials, plus the resistance caused by current collectors and interconnects, and contact resistances. Ohmic polarization is directly proportional to current density, and is affected by cell geometry, selection of the materials, and operation temperature. Upon neglecting the interaction resistances and from the ohm's law, the ohmic polarization can be calculated as:

$$\Delta V_{ohm} = iR_{ohm} \tag{4}$$

where, i shows the current density, and R_{ohm} is the total internal resistance of the cell. R_{ohm} is estimated by [13]:

$$R_{ohm} = \frac{\delta_{anode}}{\sigma_{anode}} + \frac{\delta_{cathode}}{\sigma_{cathode}} + \frac{\delta_{elec}}{\sigma_{elec}} \tag{5}$$

where, δ_{anode} , $\delta_{cathode}$, and δ_{elec} are the thickness of the anode, the cathode and the electrolyte, respectively. σ_{anode}, $\sigma_{cathode}$, and σ_{elec} are the conductivity of the anode, the cathode and the electrolyte, respectively.

C. Activation polarization

To start a chemical reaction, the reactants require a specific amount of energy called activation energy ($\mathrm{E_{act}}$). In the SOFC, this activation energy is required for the conversion of molecular $\mathrm{O_2}$ into $\mathrm{O^{2-}}$ at the cathode and $\mathrm{O^{2-}}$ into oxygen containing products at the anode. The Butler–Volmer (B–V) Equation is used to calculate the activation polarization at each electrode–electrolyte interface[14]:

$$i = i_0(e^{\alpha_1(F/RT)\Delta V_{act}} - e^{-\alpha_2(F/RT)\Delta V_{act}}) \tag{6}$$

where, i is the current density; i_0 is the exchange current density; α_1 and α_2 are the reduction and oxidation transfer coefficients; ΔV_{act} is the activation losses. The equilibrium exchange current density i_0, highly depends on the materials, construction, and temperature of the cell. The current density that flows equally in both directions at equilibrium is called the exchange current density. The faster the reaction, the higher the exchange current density, and vice versa. The value of i_0 can be determined by the Arrhenius-Equation [13]:

$$i_0 = Ae^{-E_{act}/RT} \tag{7}$$

The reduction and oxidation transfer coefficients, α_1 and α_2, are dictated by the process of electron transfer which takes place through the electrode–electrolyte interfaces. The pre-exponential term A also depends on the temperature of the cell, as well as the partial pressures of the reactant and product. For a hydrogen-fueled SOFC, the overall reactions at the anode and cathode are defined by:

$$H_2 + O^{2-} \longrightarrow H_2O + 2e^- \tag{8}$$

$$1/2\ O_2 + 2e^- \longrightarrow O^{2-} \tag{9}$$

Although implicit methods should be used to solve the Butler–Volmer Equation for determining the value of activation polarization, some explicit methods are available in the literature. To reduce modelling inaccuracies, it is critical to realize the applicable range of each of these explicit methods. In the case of high activation polarization $\Delta V_{act} > 200$ mV, in the B–V Equation (6), the first exponential term is substantially greater than the second term. The high-field approximation, also known as the Tafel Equation, is the result of neglecting the second exponential term. So, the value of activation losses can be estimated using the following formula:

$$\Delta V_{act} \cong \frac{RT}{\alpha_1 F} ln(\frac{i}{i_0}) \tag{10}$$

Because the hyperbolic sine function behaves similarly to the profile of the corresponding ΔV_{act} against current density curve, a hyperbolic sine function is used as an approximation to the B–V Equation. In fact, the activation loss can be determined explicitly if α_1 and α_2 are assumed to be equal:

$$\Delta V_{act} \cong \frac{RT}{\alpha_1 F} \sinh^{-1}(\frac{i}{2i_0}) \tag{11}$$

D. Concentration polarization

Concentration polarization is the result of reactant gas (either fuel or air) deficiency at the electrolyte/electrode interface. For example, the oxygen gas partial pressure in the bulk of the cathode is normally larger than the respective oxygen partial pressure at the electrolyte/cathode interface. Moreover, the value of concentration polarization can increase by increasing the current density due to increasing the rate at which reactants (fuel or air) are consumed in the vicinity of the electrolyte. The current produced in the limiting condition of mass transport, when the concentrations of reactants at the catalyst active sites decrease to zero, is known as the limiting current density i_L. The i_L is the highest current that can be pulled from the cell. The actual voltage is reduced because of reactant depletion and product buildup [13]. The mass transport limitation causing the polarization is expressed by [15]:

$$\Delta V_{con} = c\ ln(\frac{i_L}{i_L - i}) \tag{12}$$

where, c is the concentration loss constant. The constant c is expressed as:

$$c = \frac{RT}{nF} \tag{13}$$

IV. Results and discussion

According to Fig. 2 (a), the electrolyte is dense with 6.2-6.5 µm thickness. A dense electrolyte is essential for achieving an open circuit voltage (OCV) close to the theoretical value. In addition, infiltrated nanoparticles are visible inside the YSZ scaffold of the cathode in Fig. 2 (b). As can be seen from

Fig. 2 (c), cathode infiltrates are deposited onto the YSZ scaffold up to the electrolyte/cathode active interface. Due to the fine size of the infiltrates, the oxygen reduction reaction is expected to increase. Moreover, the porous YSZ scaffold is less than 10 µm to avoid concentration polarization on the cathode side. The good attachment of the electrodes (cathode or AFL) with the electrolyte in Fig. 2 (a) is important for effective ion transport from the active cathode TPBs into the bulk of the electrolyte or from the bulk of the electrolyte to the TPBs inside the AFL. The total thickness of the anode support and AFL shown in Fig. 2 (d) is about 368 µm. The porosity of the anode support and AFL following reduction were 45 and 35%, respectively, and the porosity of the cathode following infiltration was 35%. A high porosity anode support facilitates gas diffusion and removal of the reaction products. The porosity at the reaction sites of both electrodes was smaller to provide sufficient reaction points.

The validated model in Fig. 3, is used in this section to assess the effect of various design and operational factors on the SOFC performance. The performance of the SOFC at 500, 550, and 600°C was studied. The peak power density (PPD) of the cell at 500, 550 and 600°C is 85, 260 and 640 $\mathrm{mW.cm^{-2}}$ respectively. Researchers have studied SOFCs with $\mathrm{Nd_2NiO_{4+\delta}}$ infiltrated cathodes before. Laguna-Bercero et al. achieved a PPD of 400 $\mathrm{mW.cm^{-2}}$ at 600°C using a Ni-YSZ support, YSZ electrolyte and $\mathrm{Nd_2NiO_{4+\delta}}$ infiltrated YSZ scaffold [11]. Chen et al. infiltrated $\mathrm{Nd_2NiO_{4+\delta}}$ into a scandia stabilized zirconia (SSZ) scaffold and used a SSZ electrolyte and Ni-YSZ support. They achieved the a PPD of 280 $\mathrm{mW.cm^{-2}}$ at 650°C ($\mathrm{H_2}$:$\mathrm{H_2O}$ = 50:50 vol ratio) under SOFC mode [16]. They also noticed that the polarization resistance was higher when screen printed $\mathrm{Nd_2NiO_{4+\delta}}$ was used compared with infiltrated $\mathrm{Nd_2NiO_{4+\delta}}$. Dogdibegovic et al. [17] studied the performance of different infiltrated Ruddlesden-Popper cathodes including $\mathrm{Nd_2NiO_{4+\delta}}$. They could achieve a PPD of 1 $\mathrm{W.cm^{-2}}$ at 700°C using $\mathrm{Nd_2NiO_{4+\delta}}$ infiltration inside the cathode scaffold and co-infiltration of Ni and Sm-doped ceria (SDC) inside the anode scaffold of a metal-supported SOFC. The effect of changes of the current density on the cell voltage and power density is shown in Fig. 4. As can be seen, higher voltages and power densities can be achieved at higher temperatures. When the temperature increases, the slope of the activation and ohmic polarizations decrease sharply, as illustrated in Figs. 5 and 6. Both ohmic and activation polarizations increase sharply at low temperatures when the current density increases. The thermally activated dependence of the YSZ ionic conductivity causes the ohmic polarization to be temperature dependent; when the temperature drops, the ohmic resistance rises and vice versa. At lower temperatures, the kinetics of the electrochemical reactions slows down which leads to an increase in activation polarization. Therefore, lowering the electrolyte thickness, as well as increasing the TPB length (by infiltration of nano-size infiltrates) of an active cathode and having finer Ni and YSZ grains in the AFL, would enable the operation temperature to be lowered. Additionally, maximum current density is greater at higher temperatures due to an increase in the rate of the electrochemical reactions.

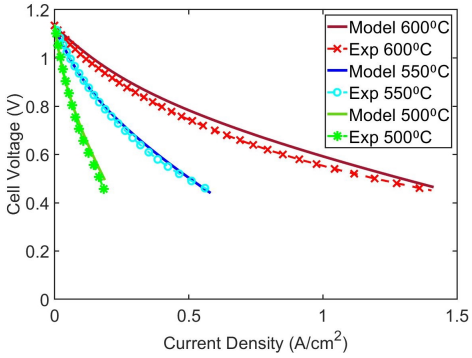

Fig. 3. Comparison between experimental and simulated results for the studied SOFC.

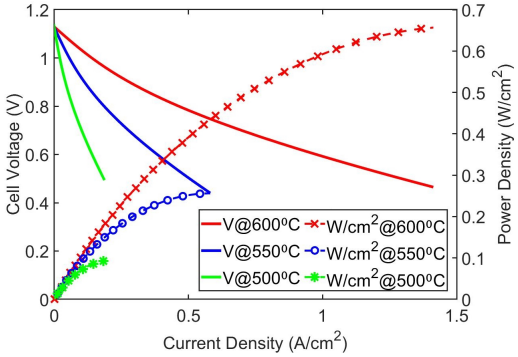

Fig. 4. Voltage and power density vs. current density at different operating temperature 500, 550 and 600 °C.

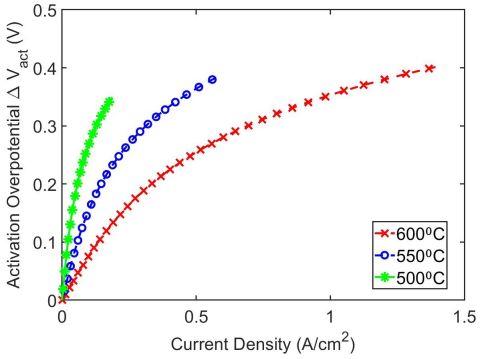

Fig. 5. Effect of operating temperature on activation overpotential.

The concentration overpotential, unlike the activation and ohmic overpotentials, increases as the temperature rises as shown in Fig. 7. However, when compared to the effects of activation and ohmic overpotentials on the SOFC performance, the difference in the concentration due to varying the operation temperature is negligible. Lowering the operation temperature would reduce the cell performance due to an increase of

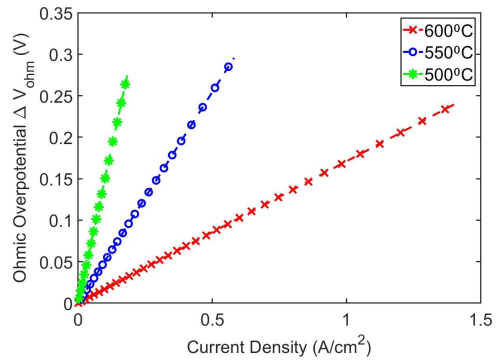

Fig. 6. Effect of operating temperature on ohmic overpotential.

different resistances; however, it would also enable the use of more common and less costly materials in manufacturing some fuel cell components and more importantly improves the cell stability.

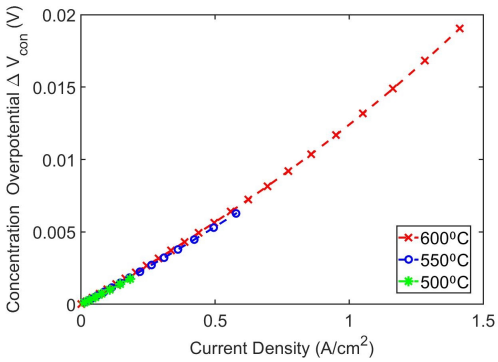

Fig. 7. Effect of operating temperature on concentration overpotential.

V. Conclusions

High operation temperature ($>$ 650°C) which leads to an increase of the degradation rate has limited the widespread use of SOFCs. In order to lower the operation temperature, a novel anode-supported tubular cell was developed. Building the cathode with nano-size infiltrated particles with high catalytic activity and ionic porous pathways, along with a thin and dense YSZ electrolyte, an active anode functional layer and a porous Ni-YSZ support, resulted in a new cell that shows high performance at low temperatures. After validating the developed model with experimental data, a parametric analysis was performed to investigate the effect of cell operation temperature and current density on different polarizations polarizations, cell voltage, and power density. The important findings are listed below:

- Simulation is a powerful tool in designing the fuel cell configuration for operation at low temperatures.
- According to the simulation and experimental results, activation polarizations and ohmic polarizations are the dominant polarizations in the cell. Due to the low thickness of the electrolyte and also the presence of an infiltrated $Nd_2NiO_{4+\delta}$ cathode and fine Ni and YSZ grains in the AFL, the novel cell developed shows low ohmic and activation polarizations at low temperatures which led to its superb performance.
- The higher the operation temperature of the cell, the higher the cell voltage at constant current density, resulting in higher power densities. In this regard, the maximum power density of 0.1, 0.25, and 0.66 W/cm^2 can be achieved at 500, 550, and 600°C, respectively.

Future study will include model-based optimization of an SOFC stack using the developed cells. Future work will also include developing and testing the SOFC stack, as well as coupling the stack with waste heat recovery units for improving its efficiency and economic feasibility.

References

[1] Nabat MH, Soltani M, Razmi AR, Nathwani J, Dusseault MB. Investigation of a green energy storage system based on liquid air energy storage (LAES) and high-temperature concentrated solar power (CSP): Energy, exergy, economic, and environmental (4E) assessments, along with a case study for San Diego, US. Sustain Cities Soc 2021;75:103305. doi:doi.org/10.1016/j.scs.2021.103305.

[2] EA, Net Zero by 2050 A Roadmap for the Global Energy Sector, (2021) 222. https://www.iea.org/reports/net-zero-by-2050. n.d.

[3] Min G, Park YJ, Hong J. 1D thermodynamic modeling for a solid oxide fuel cell stack and parametric study for its optimal operating conditions. Energy Convers Manag 2020;209:112614. doi:10.1016/j.enconman.2020.112614.

[4] Liu Y, Shao Z, Mori T, Ping S. Development of nickel based cermet anode materials in solid oxide fuel cells – Now and future. Mater Reports Energy 2021:100003. doi:10.1016/j.matre.2020.11.002.

[5] Xu H, Chen B, Tan P, Xuan J, Maroto-valer MM, Farrusseng D. Modeling of all-porous solid oxide fuel cells with a focus on the electrolyte porosity design. Appl Energy 2019;235:602–11. doi:10.1016/j.apenergy.2018.10.069.

[6] Chen X, Lin J, Sun L, Liu T, Wu J, Sheng Z, et al. Improvement of output performance of solid oxide fuel cell by optimizing the active anode functional layer. Electrochim Acta 2019;298:112–20. doi:10.1016/j.electacta.2018.12.078.

[7] Haslam JJ, Pham A, Chung BW, Dicarlo JF, Glass RS. Effects of the Use of Pore Formers on Performance of an Anode Supported Solid Oxide Fuel Cell. J Am Ceram Soc 2005;518:513–8. doi:10.1111/j.1551-2916.2005.00097.x.

[8] Ma J, Yan M, Zhang Y, Qin S. Analysis of mass transport in solid oxide fuel cells using a thermodynamically consistent model. Int J Energy Res 2021:1–11. doi:10.1002/er.7586.

[9] Man S, Jeong A, Hyun J, Kim C, Sofc A. Three-dimensional micro/macroscale simulation of planar, anode-supported, intermediate-temperature solid oxide fuel cells: I. Model development for hydrogen fueled operation. Int J Hydrogen Energy 2019;44:15456–81. doi:10.1016/j.ijhydene.2019.04.183.

[10] Hanifi AR, Laguna-Bercero MA, Sandhu NK, Etsell TH, Sarkar P. Tailoring the Microstructure of a Solid Oxide Fuel Cell Anode Support by Calcination and Milling of YSZ. Sci Rep 2016;6:27359. https://doi.org/10.1038/srep27359.

[11] Laguna-Bercero MA, Hanifi AR, Monzón H, Cunningham J, Etsell TH, Sarkar P. High performance of microtubular solid oxide fuel cells using $Nd_2NiO_{4+\delta}$-based composite cathodes. J Mater Chem A 2014;2:9764–70. https://doi.org/10.1039/c4ta00665h.

[12] Yang S, Chen T, Wang Y, Peng Z, Wang WG. Electrochemical analysis of an anode-supported SOFC. Int. J. Electrochem. Sci. 2013 Feb 1;8(2):2330-44.

[13] O'hayre R, Cha SW, Colella W, Prinz FB. Fuel cell fundamentals. John Wiley & Sons; 2016 May 2.

[14] Noren DA, Hoffman MA. Clarifying the Butler–Volmer equation and related approximations for calculating activation losses in solid oxide fuel cell models. Journal of Power Sources. 2005 Dec 1;152:175-81.

[15] Haji S. Analytical modeling of PEM fuel cell i–V curve. Renewable Energy. 2011 Feb 1;36(2):451-8.

[16] T. Chen, M. Liu, C. Yuan, Y. Zhou, X. Ye, Z. Zhan, C. Xia, S. Wang, High performance of intermediate temperature solid oxide electrolysis cells using $Nd_2NiO_{4+\delta}$ impregnated scandia stabilized zirconia oxygen electrode, J. Power Sources. 276 (2015) 1–6. https://doi.org/10.1016/j.jpowsour.2014.11.042.

[17] E. Dogdibegovic, R. Wang, G.Y. Lau, M.C. Tucker, High performance metal-supported solid oxide fuel cells with infiltrated electrodes, J. Power Sources. 410–411 (2019) 91–98. https://doi.org/10.1016/j.jpowsour.2018.11.004.